

ANALYZING THE LOCATION OF TC RAIN BANDS RELATIVE TO THE STORM CENTER USING METRICS OF DISPERSION AND CLOSURE FOR CHANGES IN RADIAL AND TANGENTIAL DIRECTIONS

1488

Corene J. Matyas¹ *, Jingyin Tang²

¹University of Florida, Gainesville, Florida; ²The Weather Company/ IBM, Atlanta, GA

1. INTRODUCTION

The rainfall produced by tropical cyclones (TCs) can cause devastating floods as during Hurricanes Harvey (2017) and Florence (2018). Many studies limit TC rainfall comparisons to calculation of areal coverage of rain rates, but this does not provide information about the spatial arrangement of the rain rates. Configurations of TC rain fields can vary according to environmental conditions and storm attributes. It is important to track their evolution so that different model projections can be compared. Weakening after landfall, increasing vertical wind shear, reductions in moisture, and baroclinic interactions should lead to less rainfall surrounding the circulation center (decreasing closure), and spreading of rainfall away from the storm center (increasing dispersion).

We compare rainband configurations for three U.S.-landfalling major hurricanes: Jeanne (2004), Harvey (2017), and Florence (2018). Although they all transitioned into extratropical cyclones (Table 1), their landfall locations (Fig. 1), sizes, rates of de-intensification differed. Jeanne and Harvey reached their maximum intensity near landfall time, and weakened to tropical storm intensity 12-14 hours after landfall. Florence had reached its maximum intensity more than 2 days prior to landfall, but weakened to a tropical storm in a similar timeframe: 13 hours after landfall. Jeanne weakened to a tropical depression first, while Harvey took nearly 5 days to do so. Jeanne and Florence were declared post-tropical about 3 days post-landfall, while it took 144 hours for Harvey to finish its transformation. According to the extended best track dataset (Demuth et al. 2006), they had a similar radius of outermost closed isobar at landfall, although Jeanne was increasing (Fig. 2). However, the quadrant-averaged radius of tropical storm-force winds (Fig. 3) was more similar for Florence and Jeanne, while Harvey had the smallest values.

* Corresponding author address:
Corene J. Matyas, Univ. of Florida, Dept. of Geography, Gainesville, FL 32611-7315; e-mail matyas@ufl.edu

Table 1. Time of landfall and the number of hours after landfall for key intensity thresholds.

Event	Jeanne	Harvey	Florence
Landfall	2004-09-26 0400	2017-08-26 0600	2018-09-16 1115
Max. Intensity	0	-3	-65
Tropical Storm	14	12	13
Tropical Depression	38	114	55
Post Tropical	68	144	73

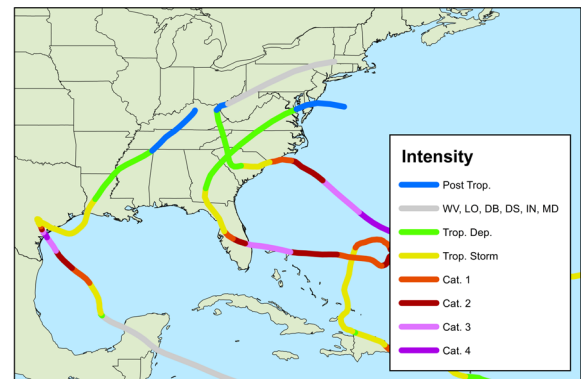


Fig. 1 Tracks of Harvey, Jeanne, and Florence with color indicating intensity.

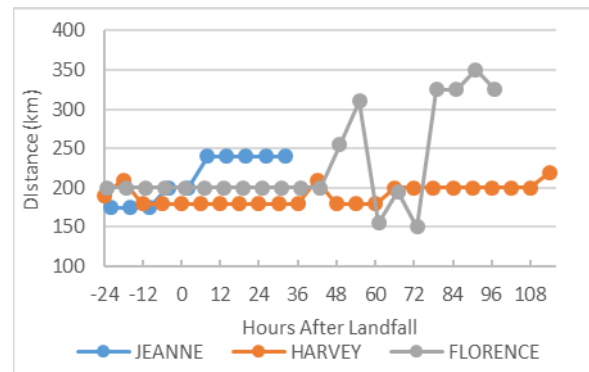


Fig. 2. Radius of outermost closed isobar beginning 24 hours before landfall.

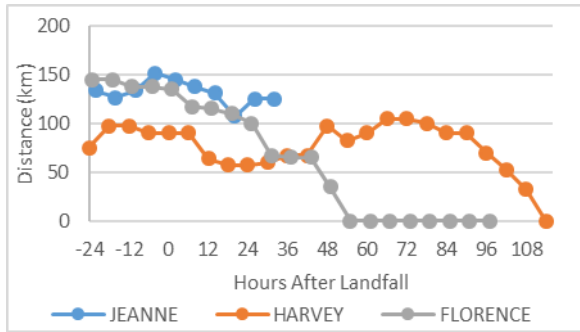


Fig. 3. Quadrant-averaged radius of gale-force winds beginning 24 hours before landfall.

As weakening of the primary and secondary circulations in a TC should correspond to decreases in rainband activity in the tangential and increases in the radial directions relative to the storm center, we calculate closure and dispersion for stratiform (20 dBZ) and convective (40 dBZ) regions detected by the WSR-88D network and compare rates of change in these storms. We also average the extent of 20 dBZ regions in each quadrant to determine the search radius needed and when rainbands are within radar range.

2. DATA AND METHODS

The first task is to create a 3D grid of reflectivity values. Jeanne (2004) occurred during the legacy period of the WSR-88D network (OFCM 2006), while Harvey and Florence were sampled more recently using dual-polarization (OFCM 2017). We process Level II reflectivity data (NOAA 1991) from WSR-88D stations within 600 km of the storm center. Using techniques described in Tang and Matyas (2016), we pre-process, convert to a Cartesian grid, and perform interpolations when necessary to create gridded reflectivity values at a 1 km x 1 km 1 0.5 km resolution using data from a 10-minute moving window. Values for grid cells with data from multiple radars retain the highest reflectivity value. Cells with missing values are filled using a distance-weighted interpolation. Data are gridded every 10 minutes. The grid extends to 750 km from the storm's center, which is interpolated from the best track using splines to a 10-minute resolution. For this study, we utilize a data at 3 km altitude above sea level.

We employ a Geographic Information System (GIS) to identify regions containing specific reflectivity values every 10 minutes. First, we identify the boundaries of reflectivity

values every 5 dBZ by drawing contour lines. These contour lines are converted into polygon shapes (Fig. 4) so that each shape has a perimeter that is defined by the edge of the given reflectivity value, but contains values equal to or greater than this value. Calculations of area and geographical centroid as well as the distance and bearing to the storm's center are performed. Only polygons with centroids located within 500 km of the storm center are included (Jiang et al. 2011)

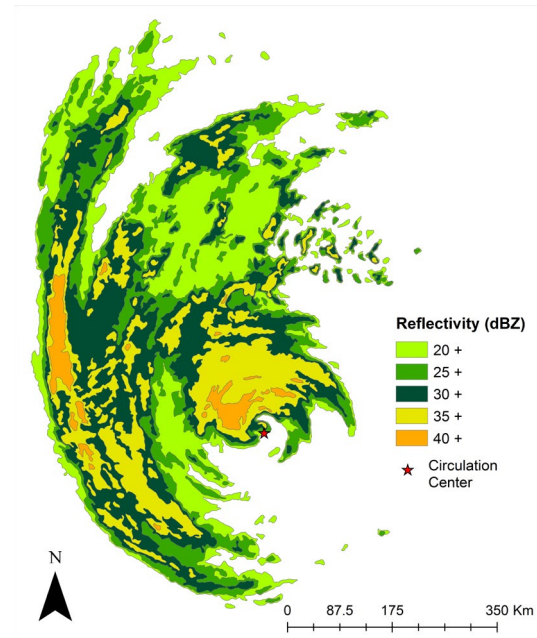


Fig. 4 Reflectivity polygons every 5 dBZ.

a. Spatial metric calculations

Changes in the shape, and location of the TC rain field relative to its circulation center occur as a TC moves inland and interacts with the relatively dry continental air mass and/or while transforming from a warm-cored system into a cold-cored extratropical cyclone (Klein et al. 2000; Atallah et al. 2007; Matyas 2007; Peng et al. 2007; Matyas 2010; Xu et al. 2014; Zick and Matyas 2016). Thus, the spatial arrangement of the TC's rainbands should evolve from a compressed shape enclosing the storm center to a shape that becomes more spread out with reflectivity regions that do not fully encircle the storm center. The metrics that we calculate are closure and dispersion.

Similar to the rain shield arc length calculated in Matyas (2007), *closure* measures the distribution of reflectivity in the azimuthal

direction. The presence of reflectivity is evaluated at each 1° angle and the number of intersections is divided by 360 to obtain a value in the 0-1 range. *Dispersion* (Massam and Goodchild 1971) measures the radial distribution of precipitation, with small values indicating that the mass of precipitation is close to the center. Dispersion increases to a value of one as the reflectivity region centroid(s) ($r_{centroid}$) move radially away from the circulation center and have their centroids located at the edge of the search radius (r_{search}). Each reflectivity region is weighted by its area, and the final metric is calculated by summing over all reflectivity regions, with NP representing the number of polygons. We scale each to the range 0-1 and name them so that larger values match the descriptive term (Fig. 5).

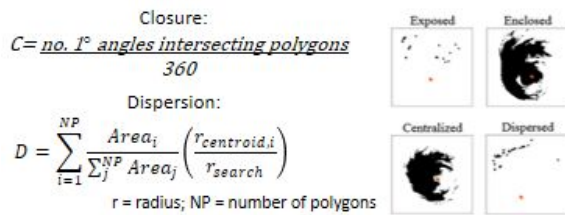


Fig. 5 Two spatial metrics, their equations, and examples of low and high-end shapes.

For closure, we set an exclusion zone of 50 km around the storm center to account for errors in the spline interpolation of the storm center. Dispersion requires a search radius to establish its outermost bounds where if all polygon centroids were located at this distance, the metric would equal one. We determine this distance objectively by calculating how far out reflectivity polygons extend from the storm center in each quadrant of the storm. At each 1° interval around the storm center, the extent of reflectivity is measured, and these are averaged over northeast, southeast, southwest, and northwest quadrants in a manner similar to that used in the extended best track (Fig. 6). We examine these values to determine the maximum distance over which reflectivity could occur for each storm. We use this same search radius for closure. Plots of rain field extent also help determine when analysis can commence as values increase when the TC is moving into radar range. All three of these TCs moved into range from the east, so values will increase sharply in the northeast and/or southeast

quadrants until the entire TC is within range of the radars.

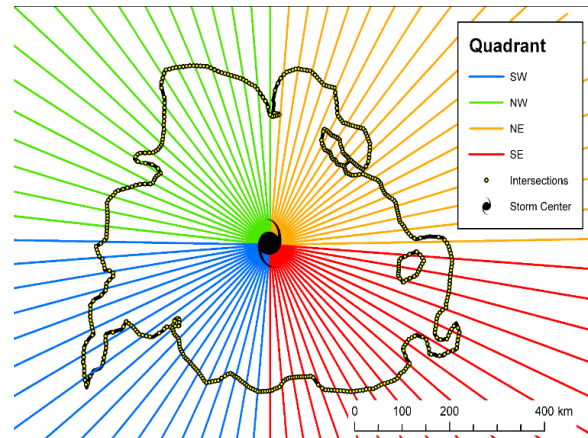


Fig. 6. Measuring reflectivity extent and averaging for each quadrant. These lines are spaced every 5° for easy viewing.

For brevity, we only present the result of two reflectivity thresholds. We select reflectivity values of 20 dBZ to represent light rainfall. Many researchers have used this threshold to define the edge of a TC (e.g., Jorgensen 1984; Matyas 2007; Hazelton and Hart 2013). As in previous research (Jorgensen 1984; Steiner et al. 1995; Skwira et al. 2005; Matyas 2009; Matyas 2010), we select 40 dBZ to represent higher rain rates associated with convective precipitation.

3. RESULTS

3.1 Determination of search radius and analysis start time

As the analysis for Jeanne could only begin 4 hours prior to landfall (Fig. 7a), we selected this time as the point of commencement for all three TCs. We line up our results according to hours after landfall to facilitate comparisons. Jeanne's extent increased in the northeast quadrant, decreased in the southwest, and was fairly steady in the southeast. As values never exceeded 450 km, we set this distance as the search radius for Jeanne. The northeast quadrant had the largest extent over all for the three TCs. Harvey's extent was the farthest (Fig. 7b), so we set its search radius as 500 km, and choose 450 km for that of Florence (Fig. 7c).

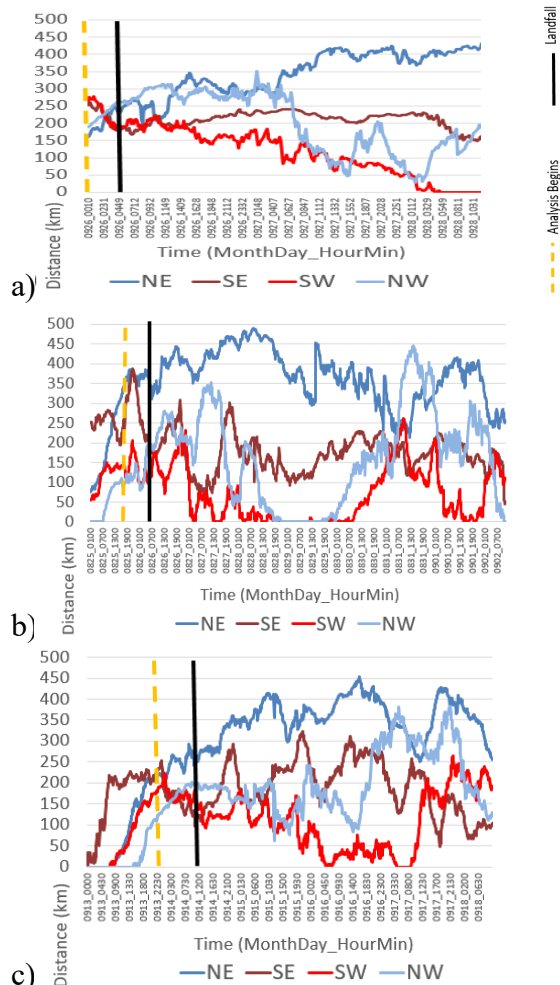


Fig. 7. Extent of 20 dBZ regions from center in each quadrant for a) Jeanne, b) Harvey, and c) Florence.

3.2 Examples of metrics at landfall and 36 hours post-landfall

We present images of reflectivity values every 5 dBZ (Fig. 8) to visualize the mosaics that we created and compare the metric values at the time of landfall. Jeanne has a large eye and contains good coverage of 35 dBZ regions, and a large region of 40 dBZ values appears on its south side. The outer rainbands are fragmented and thus represent only small areas in the calculation of the dispersion metric. Thus, Jeanne is the most compressed of the three TCs at this time in both 20 and 40 dBZ values (Table 2). All TCs centers are completely enclosed by 20 dBZ regions, but 40 dBZ values enclose a larger percentage of Jeanne's center and thus, it has the highest closure value. Harvey has the highest dispersion of 20 dBZ values due to the

rainfall region that extends far north of center. Harvey and Florence have more 40 dBZ regions in their outer rainbands, leading to larger dispersion values.



Fig. 8. At landfall, reflectivity at 3 km for a) Jeanne, b) Harvey, and c) Florence.

Table 2. Metric values for each storm at the time of landfall.

Metric	Jeanne	Harvey	Florence
Dispersion 20 dBZ	0.15	0.23	0.19
Dispersion 40 dBZ	0.29	0.34	0.38
Closure 20 dBZ	1.00	1.00	1.00
Closure 40 dBZ	0.31	0.12	0.14

To illustrate our methods, at 36 hours post-landfall, we present only the regions enclosed by 20 and 40 dBZ from which the metrics are calculated (Fig. 9). Jeanne is the weakest TC and has the least convection (Fig. 9a), which explains the low closure value for 40 dBZ regions (Table 3). Harvey is the most dispersed and has the most exposure for 20 dBZ regions as its rain fields are mainly northeast of center and comprise a very large area (Fig. 9b). Florence has a well-developed 40 dBZ region 250 km from center (Fig. 9c), thus it is the least dispersed as the majority of regions in Harvey and Jeanne are >400 km from center.



Fig. 9. At 36 h post-landfall, polygons enclosing 20 dBZ (green) and 40 dBZ (orange) for a) Jeanne, b) Harvey, and c) Florence. Circulation center is the black dot.

Table 3. Metric values for each storm at 36 hours post-landfall.

Metric	Jeanne	Harvey	Florence
Dispersion 20 dBZ	0.39	0.57	0.38
Dispersion 40 dBZ	0.84	0.79	0.51
Closure 20 dBZ	0.69	0.67	0.78
Closure 40 dBZ	0.03	0.12	0.16

3.3 Comparison of metric values over time

Fig. 10 shows how the values of dispersion and closure differed for each TC over time and across reflectivity values. Data are aligned by the time of landfall. Dispersion of 20 dBZ regions showed a remarkable similarity in slope (Fig. 10a). Although Harvey remained more dispersed than the other TCs, dispersion increased at a rate of ~ 4 km per hour. The R^2 value of this slope is >0.89 . Total increases in dispersion were 180-220 km. Reflectivity regions bounded by 20 dBZ values no longer completely enclosed the circulation center at 19 h post-landfall for Jeanne and Harvey, and 24 h post-landfall for Florence. This is about 6-12 h after weakening to tropical storm intensity. Matyas et al. (2018) calculated dispersion and closure of 20 dBZ regions for Hurricane Isabel (2003) during its extratropical transition and found a fairly steady rate of exposure for 20 dBZ values of 16.5° per hour, with opening beginning 3 h after landfall. Its rate of dispersion was slower at 3.2 km/hr.

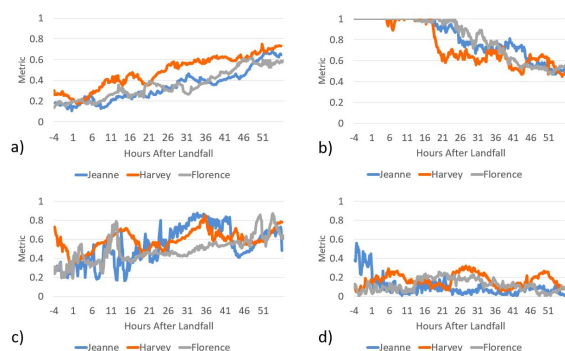


Fig. 10 a) Dispersion of 20 dBZ, b) closure of 20 dBZ, c) dispersion of 40 dBZ, d) closure of 40 dBZ regions with search radius of 50-450 km (Jeanne and Florence) and 50-500 km (Harvey).

20 dBZ values no longer completely encircled the center at 19 hours post-landfall for Jeanne and Harvey, but 24 hours post-landfall for Florence (Fig. 10b). This is about 6 to 12 hours after weakening to tropical storm intensity. Once values began to decline, 20 dBZ closure decreased at 4.1° and 5.4° per hour for Jeanne and Florence, with R^2 values > 0.86 . Values bottomed out around 180° .

The dispersion of the 40 dBZ regions saw more variability within and among the three TCs, although the overall trend was for increasing values (Fig. 10c). Harvey had the most smooth pattern and tended to be the most dispersed for the first 18 hours. At that point, Jeanne was the most dispersed over the next 30 hours as 40 dBZ regions eroded from the main rain shield and only occurred in the outer rainband to the east of center. The formation and dissipation of 40 dBZ regions near the storm center caused the high variability seen in its dispersion values during the first 18 hours after landfall. From 18-43 hours post-landfall, Florence had the smallest and least-varying dispersion values. In terms of closure, 40 dBZ regions were dispersed in the outer rainbands, which limits tangential extent (Fig. 10d). The large arc of higher reflectivity surrounding Jeanne's center near landfall can be seen to dissipate within the first five hours and after this, Jeanne has the lowest closure of 40 dBZ values overall. Average closure values for Jeanne were 10% and 12% for Florence, Harvey was highest at 17%.

4. FUTURE RESEARCH

Prior to the Annual Meeting, data from the Statistical Hurricane Intensity Prediction Scheme (SHIPS) (DeMaria et al. 2005) were not available for the 2018 season. Data were utilized to compare atmospheric conditions for Jeanne and Harvey to better understand differences in rain field evolution. For brevity, only deep-layer (200-850 hPa) vertical wind shear and total precipitable water averaged for two different storm-relative regions were examined. As lags of 12-24 hours have been found between environmental conditions and rain field evolution (Frank and Ritchie 2001; Wingo and Cecil 2010; Matyas 2013; Zhou et al. 2018), we examine data beginning 48 hours before landfall. Future research will examine atmospheric conditions more thoroughly for all three TCs.

Before landfall, vertical wind shear speed increased for both Jeanne and Harvey, but Harvey (average 7 m/s) experienced stronger shear than Jeanne (average 3 m/s). For Harvey, the shear vector was more consistently from the southwest (245°), which could account for more dispersion towards the northeast. After landfall, shear increased across Jeanne, averaging 12.8 m/s from 229°. During the same period, shear was fairly similar across Harvey, averaging 12.4 m/s from 247°.

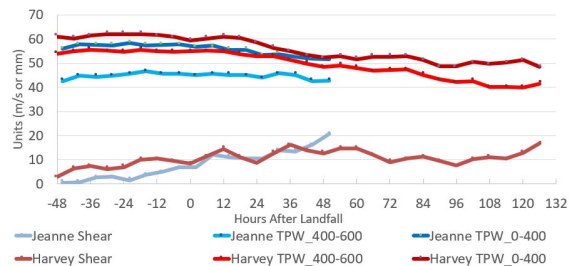


Fig. 11 Values of 200-850 hPa wind shear velocity and total precipitable water averaged 0 – 400 and 400-600 km from storm center for Jeanne (blue) and Harvey (red).

Total precipitable water averaged inside of 400 km provides a measure of moisture within the storm. Data averaged over an annulus 400-600 km away from storm center provides information about the amount of moisture available outside of the storm. Both variables showed that more moisture was available for Harvey than Jeanne. While values inside of the storm averaged 55 and 59 mm, outside of the storm, Harvey averaged 10 mm more than Jeanne. This could have limited the development of outer rainbands in Jeanne, leading to less dispersion near landfall. With increasing vertical wind shear, it could also have limited the supply of moisture to sustain deep convection so that little 40 dBZ regions existed as the ET process proceeded.

5. ACKNOWLEDGEMENTS

This research was funded the National Science Foundation BCS-1053864, which ended in 2018.

6. REFERENCES

Atallah, E. H., L. F. Bosart, and A. R. Aiyer, 2007: Precipitation distribution associated with

landfalling tropical cyclones over the eastern United States. *Mon. Wea. Rev.*, **135**, 2185-2206.

Center, N. N. W. S. N. R. O., 1991. NOAA Next Generation Radar (NEXRAD) Level II Base Data. NOAA National Centers for Environmental Information. [Available online at <https://www.ncdc.noaa.gov/nexradinv/>.] Accessed 10 February 2016.

DeMaria, M., M. Mainelli, L. K. Shay, J. A. Knaff, and J. Kaplan, 2005: Further improvements to the Statistical Hurricane Intensity Prediction Scheme (SHIPS). *Wea. Forecasting*, **20**, 531-543.

Demuth, J. L., M. DeMaria, and J. A. Knaff, 2006: Improvement of advanced microwave sounding unit tropical cyclone intensity and size estimation algorithms. *J. Appl. Meteorol. Climatol.*, **45**, 1573-1581.

Frank, W. M., and E. A. Ritchie, 2001: Effects of vertical wind shear on the intensity and structure of numerically simulated hurricanes. *Mon. Wea. Rev.*, **129**, 2249-2269.

Hazelton, A. T., and R. E. Hart, 2013: Hurricane eyewall slope as determined from airborne radar reflectivity data: Composites and case studies. *Wea. Forecasting*, **28**, 368-386.

Jiang, H., C. Liu, and E. J. Zipser, 2011: A TRMM-based tropical cyclone cloud and precipitation feature database. *J. Appl. Meteorol. Climatol.*, **50**, 1255-1274.

Jorgensen, D. P., 1984: Mesoscale and convective-scale characteristics of mature hurricanes. Part I: General observations by research aircraft. *J. Atmos. Sci.*, **41**, 1268-1285.

Klein, P. M., P. A. Harr, and R. L. Elsberry, 2000: Extratropical transition of western North Pacific tropical cyclones: An overview and conceptual model of the transformation stage. *Wea. Forecasting*, **15**, 373-395.

Massam, B. H., and M. F. Goodchild, 1971: Temporal trends in the spatial organization of a service agency. *The Canadian Geographer/Le Géographe canadien*, **15**, 193-206.

- Matyas, C. J., 2007: Quantifying the shapes of US landfalling tropical cyclone rain shields. *The Professional Geographer*, **59**, 158-172.
- Matyas, C. J., 2009: A spatial analysis of radar reflectivity regions within Hurricane Charley (2004). *J. Appl. Meteorol. Climatol.*, **48**, 130-142.
- Matyas, C. J., 2010: A geospatial analysis of convective rainfall regions within tropical cyclones after landfall. *International Journal of Applied Geospatial Research*, **1**, 69-89.
- Matyas, C. J., 2013: Processes influencing rain-field growth and decay after tropical cyclone landfall in the United States. *J. Appl. Meteorol. Climatol.*, **52**, 1085-1096.
- Matyas, C. J., S. E. Zick, and J. Tang, 2018: Using an object-based approach to quantify the spatial structure of reflectivity regions in Hurricane Isabel (2003): Part I: Comparisons between radar observations and model simulations. *Mon. Wea. Rev.*, **146**, 1319-1340.
- OFCM, 2006: Federal Meteorological Handbook, No. 11: Doppler Radar Meteorological Observations. Part D, WSR-88D unit description and operational applications. U.S. Department of Commerce, 1-218.
- OFCM, 2017: *Federal Meteorological Handbook, No. 11: WSR-88D Meteorological Observations. Part C WSR-88D Products and Algorithms*. U.S. Department of Commerce/ NOAA.
- Peng, M. S., R. N. Maue, C. A. Reynolds, and R. H. Langland, 2007: Hurricanes Ivan, Jeanne, Karl (2004) and mid-latitude trough interactions. *Meteorol. Atmos. Phys.*, **97**, 221-237.
- Skwira, G. D., J. L. Schroeder, and R. E. Peterson, 2005: Surface observations of landfalling hurricane rainbands. *Mon. Wea. Rev.*, **133**, 454-465.
- Steiner, M., R. A. Houze, and S. E. Yuter, 1995: Climatological characterization of 3-dimensional storm structure from operational radar and rain-gauge data. *J. Appl. Meteor.*, **34**, 1978-2007.
- Tang, J., and C. J. Matyas, 2016: Fast playback framework for analysis of ground-based Doppler radar observations using Map-Reduce technology. *Journal of Atmospheric and Oceanic Technology*, **33**, 621-634.
- Wingo, M. T., and D. J. Cecil, 2010: Effects of vertical wind shear on tropical cyclone precipitation. *Mon. Wea. Rev.*, **138**, 645-662.
- Xu, W., H. Jiang, and X. Kang, 2014: Rainfall asymmetries of tropical cyclones prior to, during, and after making landfall in South China and Southeast United States. *Atmos. Res.*, **139**, 18-26.
- Zhou, Y., C. Matyas, H. Li, and J. Tang, 2018: Conditions associated with rain field size for tropical cyclones landfalling over the Eastern United States. *Atmospheric Research*, **214**, 375-385.
- Zick, S. E., and C. J. Matyas, 2016: A shape metric methodology for studying the evolving geometries of synoptic-scale precipitation patterns in tropical cyclones. *Annals of the Association of American Geographers*, **106**, 1217-1235.